International Journal of Heat and Mass Transfer 52 (2009) 2379–2389

Contents lists available at ScienceDirect

International Journal of Heat and Mass Transfer

journal homepage: www.elsevier.com/locate/ijhmt

A hyperbolic microscopic model and its numerical scheme for thermal analysis in an *N*-carrier system

Weizhong Dai *

Department of Mathematics and Statistics, College of Engineering and Science, Louisiana Tech University, Ruston, LA 71272, USA

ARTICLE INFO

Article history:
Received 8 May 2008
Received in revised form 10 October 2008

ABSTRACT

We extend the concept of the well-known hyperbolic two-step model for micro heat transfer to the case of energy exchanges in a generalized *N*-carrier system. The model satisfies an energy estimate and hence is well-posed. Based on this result, a finite difference scheme is developed for solving the hyperbolic microscopic model. The scheme is shown to satisfy a discrete analogue of the energy estimate, implying that it is unconditionally stable. Finally, the scheme is tested by an example. The difference between the hyperbolic model and the corresponding parabolic model for a multi-carrier system is also compared.

1. Introduction

Energy exchange between electrons and phonons in metal provides the best example in describing non-equilibrium heating during the ultrafast transient [1–6]. In times comparable to the thermalization and relaxation times of electrons and phonons, which are in the range of a few to several tens of picoseconds, heat continuously flows from hot electrons to cold phonons through mutual collisions. Consequently, electron temperature continuously decreases whereas phonon temperature continuously increases until thermal equilibrium is reached. Intensity of heat flow during non-equilibrium heating is proportional to the temperature difference between electrons and phonons. The proportional constant is termed the electron–phonon coupling factor, which is a new thermophysical property in microscale heat transfer. The mathematical equations for describing the non-equilibrium heating can be expressed as the well-known parabolic two-step model [3,4]:

$$C_e\frac{\partial T_e(\vec{x},t)}{\partial t}=k_e\nabla^2T_e(\vec{x},t))-G[T_e(\vec{x},t)-T_l(\vec{x},t)]+Q(\vec{x},t), \tag{1}$$

$$C_l\frac{\partial T_l(\vec{x},t)}{\partial t}=G[T_e(\vec{x},t)-T_l(\vec{x},t)], \tag{2}$$

where T_e and T_l are electron temperature and lattice temperature, respectively; C_e and C_l are heat capacities, k_e is the conductivity, G is the electron–phonon coupling factor, and Q is the heat source.

The same concept has been extended to model pulsed heating on amorphous media [6] and non-equilibrium heat transport in porous media [7]. In place of electrons and phonons, energy coupling between the solid and fluid/gaseous phases was described in the same way. The thermalization and relaxation times for slow materials, such as lightly packed copper spheres or rough carbon surfaces [6,8], can reach several tenths of a millisecond due to the low-conducting phases involved in the assemblies. Transient times on the order of 10^{-4} s, therefore, are considered to be ultrafast because of the pronounced thermalization and relaxation behaviors observed in the sub-millisecond domain.

Although the above coupled Eqs. (1) and (2) have been widely applied in analysis of microscale heat transfer [1–19], it has been pointed out that when the characteristic heating time (which is either the laser pulse duration or the time needed to heat a material to a certain temperature) is much shorter than the electron relaxation time of free electrons (the mean time for electrons to change their states) in a metal, the parabolic two-step model may be inadequate to describe the continuous energy flow from hot electrons to lattices during non-equilibrium heating (see Fig. 1 in [9]). Tien and Qiu [4] developed the hyperbolic two-step heat transport equations based on the macroscopic averages of the electric and heat currents carried by electrons in the momentum space. Al-Nimr et al. [20–24] also studied the thermal behavior of thin films using the hyperbolic two-step model. Chen et al. [25,26] proposed a generalized hyperbolic two-step model for studying ultrashort laser pulse interactions with metal films:

$$C_e\frac{\partial T_e}{\partial t}=-\nabla\cdot\vec{q}_e-G(T_e-T_l)+Q, \tag{3}$$

$$\tau_e\frac{\partial\vec{q}_e}{\partial t}+\vec{q}_e=-k_e\nabla T_e, \tag{4}$$

$$C_l\frac{\partial T_l}{\partial t}=-\nabla\cdot\vec{q}_l+G(T_e-T_l), \tag{5}$$

$$\tau_l\frac{\partial\vec{q}_l}{\partial t}+\vec{q}_l=-k_l\nabla T_l, \tag{6}$$

where $\vec{q}_e$ and $\vec{q}_l$ are the heat fluxes associated with electrons and the lattice, respectively, and k_l is the lattice thermal conductivity. Here, τ_e is the electron relaxation time and τ_l is the lattice relaxation time.

* Tel.: +1 318 257 3301; fax: +1 318 257 2562.
E-mail address: dai@coes.latech.edu

0017-9310/$ - see front matter © 2008 Elsevier Ltd. All rights reserved.
doi:10.1016/j.ijheatmasstransfer.2008.10.018

Nomenclature

C_1, C_e, C_l, C_j, C_N	heat capacity
E_j	difference in temperature related to carrier j
G_{ij}, G	carrier i – carrier j coupling factor
k_e, k_i, k_l	thermal conductivity
L	length of interval
M	number of grid points
N	number of carriers
Q, Q_j	heat source
$q_e, q_j, q_l, \vec{q}_j$	heat flux
$(q_j)_m^n$	numerical solution of q_j at $(m\Delta x, n\Delta t)$
T_e, T_j, T_l	temperature
$(T_j)_m^n$	numerical solution of T_j at $\left((m-\frac{1}{2})\Delta x, n\Delta t\right)$
t, t_0	time
$x, \vec{x}$	Cartesian coordinates

Greek symbols

∇	gradient operator
$\nabla_x, \nabla_{\bar{x}}$	forward and backward finite difference operators, respectively
Δt	time increment
Δx	spatial grid size
ε_j	difference in heat source related to carrier j
Ω	interval or region
τ_e, τ_j, τ_l	relaxation time
θ_j	difference in heat flux related to carrier j

It can be seen that if τ_e, τ_l and k_l are zero, the generalized hyperbolic two-step model will reduce to the parabolic two-step model.

It has been noted that non-equilibrium heating porous media [7] already involve a more complicated system than the two-carrier (electron–phonon) system in metals. Phase change in wicked heat pipes, moreover, often involves non-equilibrium heating/energy dissipation among the solid wick, liquid, and vapor phases [27]. As extensions are made to medical applications employing femtosecond lasers [28], complexities of non-equilibrium heating further evolve due to involvement of multiple carriers in biomedical systems, including hard/soft tissues (proteins), water, and minerals at least. The ways in which thermal energy is distributed among different carriers, as well as the characteristic times dictating the intrinsic behaviors of non-equilibrium heating, play a dominant role in assuring the success of femtosecond-laser technologies.

In this article, we extend the concept, which lies in the hyperbolic two-step model, to the case of the energy exchanges in a generalized N-carrier system with heat sources as follows:

$$C_1\frac{\partial T_1(\vec{x},t)}{\partial t} = \nabla\cdot\vec{q}_1 - \sum_{i=2}^{N} G_{1i}[T_1(\vec{x},t) - T_i(\vec{x},t)] + Q_1(\vec{x},t), \tag{7a}$$

$$\tau_1\frac{\partial \vec{q}_1}{\partial t} + \vec{q}_1 = -k_1\nabla T_1, \tag{7b}$$

$$C_j\frac{\partial T_j(\vec{x},t)}{\partial t} = \nabla\cdot\vec{q}_j + \sum_{i=1}^{j-1} G_{ij}[T_i(\vec{x},t) - T_j(\vec{x},t)] - \sum_{i=j+1}^{N} G_{ji}[T_j(\vec{x},t) - T_i(\vec{x},t)]Q_j(\vec{x},t), \tag{8a}$$

$$\tau_j\frac{\partial \vec{q}_j}{\partial t} + \vec{q}_j = -k_j\nabla T_j, \quad j = 2,\ldots,N-1, \tag{8b}$$

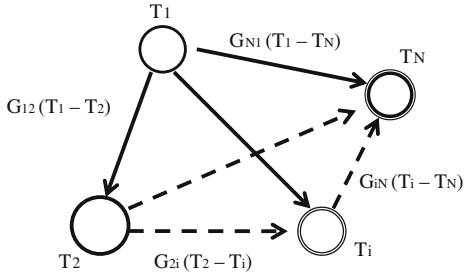

Fig. 1. Energy exchanges in a system with N carriers.

$$C_N\frac{\partial T_N(\vec{x},t)}{\partial t} = \nabla\cdot\vec{q}_N + \sum_{i=1}^{N-1} G_{iN}[T_i(\vec{x},t) - T_N(\vec{x},t)] + Q_N(\vec{x},t), \tag{9a}$$

$$\tau_N\frac{\partial \vec{q}_N}{\partial t} + \vec{q}_N = -k_N\nabla T_N; \tag{9b}$$

where T_j ($j = 1,\ldots,N$) are temperatures, C_j ($j = 1,\cdots,N$) are heat capacities, k_j ($j = 1,\ldots,N$) are conductivities, G_{ij} is the carrier i – carrier j coupling factor and positive constant, τ_j is the carrier j relaxation time, and Q_j ($j = 1,\ldots,N$) are heat sources. Here, $(\vec{x},t)$ is in $\Omega\times[0,t_0]$, where Ω is assumed to be an interval in a 1D case or a rectangular region in a 2D or 3D case. The summations with negative/positive signs in the front represent the energy lost/gained to/from other carriers. The first summation in Eq. (8a), for example, represents the volumetric energy density received by carrier j, whereas the second summation in the same equation represents the energy density released from carrier j. Non-equilibrium heating is reflected by the temperature differences in the system. Fig. 1 shows the energy exchanges among dissimilar energy carriers, which are assumed proportional to their temperature differences as that assumed during electron–phonon coupling [1–5,29]. Here, we assume that (1) different energy carriers are in perfect thermal contact, (2) the coupling factors G_{ij} only depend on the physical properties of the carriers and not on the presence (or absence) of impurities among these carriers, (3) thermal radiation exchange between these energy carriers is ignore, and (4) all N carriers are stationary in the system.

Furthermore, we assume that there are no heat losses from the system in the short time response [6]. As such, the boundary condition for $\vec{q}_j$ ($j = 1,\ldots,N$) is

$$\vec{q}_j(\vec{x},t) = 0, \quad j = 1,\ldots,N; \quad (\vec{x},t)\in\partial\Omega\times[0,t_0], \tag{10}$$

where $\partial\Omega$ is the boundary of Ω.

In the next sections, we will analyze the well-posedness of the above hyperbolic model for the generalized N-carrier system. A stable numerical method for solving the hyperbolic model will then be developed because the analytic solutions could be difficult to obtain due to a large N. Finally, the scheme will be tested by an example. The difference between the hyperbolic model and the correspondent parabolic model will also be compared.

2. Energy estimate

For simplicity, we consider the hyperbolic model,Eqs. (7–10), in one dimension and $0 \leqslant x \leqslant L$. Thus, the boundary condition can be simplified as

$$q_j(0,t) = q_j(L,t) = 0, \quad j = 1,\ldots,N. \tag{11}$$

The initial conditions are assumed to be

$$T_j(x,0)=T_j^0(x),\quad q_j(x,0)=q_j^0(x),\quad j=1,\ldots,N. \tag{12}$$

To obtain an energy estimate, we assume that all coefficients C_j, k_j, G_{ij}, τ_j are positive constants, and the solutions and the initial conditions are smooth. Multiplying Eq. (7a) by $T_1(x,t)$, Eq. (8a) by $T_j(x,t)$, and Eq. (9a) by $T_N(x,t)$, respectively, integrating them over $[0,L]$, summing the results over $1\leqslant j\leqslant N$, and performing some algebraic manipulations, we obtain

$$\int_0^L\sum_{j=1}^N C_jT_j\frac{\partial T_j}{\partial t}dx=\int_0^L\sum_{j=1}^N-\frac{\partial q_j}{\partial x}T_jdx - \int_0^L\sum_{\substack{ij=1\\ i<j}}^N G_{ij}[T_i-T_j]^2dx+\int_0^L\sum_{j=1}^N T_jQ_jdx. \tag{13}$$

The left-hand-side (LHS) of the above equation can be written as

$$\int_0^L\sum_{j=1}^N C_jT_j\frac{\partial T_j}{\partial t}dx=\frac{d}{dt}\int_0^L\frac{1}{2}\sum_{j=1}^N C_jT_j^2dx. \tag{14}$$

Using the integration by parts, the boundary condition, Eqs. (11), and (7b), (8b) and (9b), one may obtain

$$\begin{aligned}\int_0^L\sum_{j=1}^N-\frac{\partial q_j}{\partial x}T_jdx&=-\sum_{j=1}^N\int_0^L\frac{\partial q_j}{\partial x}T_jdx\\&=-\sum_{j=1}^N[T_j(L,t)q_j(L,t)-T_j(0,t)q_j(0,t)]\\&\quad+\sum_{j=1}^N\int_0^L q_j\frac{\partial T_j}{\partial x}dx\\&=\sum_{j=1}^N\int_0^L q_j\frac{\partial T_j}{\partial x}dx\\&=-\sum_{j=1}^N\int_0^L q_j\frac{1}{k_j}\left(\tau_j\frac{\partial q_j}{\partial t}+q_j\right)dx\\&=-\frac{d}{dt}\int_0^L\frac{1}{2}\sum_{j=1}^N\frac{\tau_j}{k_j}q_j^2dx-\int_0^L\sum_{j=1}^N\frac{1}{k_j}q_j^2dx.\end{aligned} \tag{15}$$

By the Cauchy–Schwarz inequality (*i.e.*,$2ab\leqslant\varepsilon a^2+\frac{1}{\varepsilon}b^2$, where $\varepsilon>0$ [30]), we obtain

$$\int_0^L\sum_{j=1}^N T_jQ_jdx\leqslant\int_0^L\frac{1}{2}\sum_{j=1}^N C_jT_j^2dx+\int_0^L\frac{1}{2}\sum_{j=1}^N\frac{1}{C_j}Q_j^2dx. \tag{16}$$

Substituting Eqs. (14)–(16) into Eq. (13) gives

$$\frac{d}{dt}\int_0^L\frac{1}{2}\sum_{j=1}^N C_jT_j^2dx+\frac{d}{dt}\int_0^L\frac{1}{2}\sum_{j=1}^N\frac{\tau_j}{k_j}q_j^2dx+\int_0^L\sum_{j=1}^N\frac{1}{k_j}q_j^2dx+\int_0^L\sum_{\substack{ij=1\\ i<j}}^N G_{ij}[T_i-T_j]^2dx\leqslant\int_0^L\frac{1}{2}\sum_{j=1}^N C_jT_j^2dx+\int_0^L\frac{1}{2}\sum_{j=1}^N\frac{1}{C_j}Q_j^2dx. \tag{17}$$

Taking out the third and fourth terms on the LHS because they are non-negative, introducing $F(t)=\int_0^L\sum_{j=1}^N[C_jT_j^2+\frac{\tau_j}{k_j}q_j^2]dx$ and $Q(t)=\int_0^L\sum_{j=1}^N\frac{1}{C_j}Q_j^2dx$, and then integrating it with respect to t, Eq. (17) can be further simplified as follows:

$$F(t)-F(0)\leqslant\int_0^t F(s)ds+\int_0^t Q(s)ds. \tag{18}$$

By Gronwall's lemma (i.e., if $\phi(t)\geqslant 0$ and $\psi(t)\geqslant 0$ are continuous functions such that $\phi(t)\leqslant K+L\int_{t_0}^t\psi(s)\phi(s)ds$ holds on $t_0\leqslant t\leqslant t_1$, where K and L are positive constants, then $\phi(t)\leqslant K\exp(L\int_{t_0}^t\psi(s)ds)$ on $t_0\leqslant t\leqslant t_1$, see [30]), we obtain for $0\leqslant t\leqslant t_0$

$$F(t)\leqslant\int_0^t 1\cdot F(s)ds+[F(0)+\int_0^t Q(s)ds]\leqslant e^t\left[F(0)+\int_0^t Q(s)ds\right], \tag{19}$$

and hence the following energy estimate for the N-carrier system can be obtained as

$$\int_0^L\sum_{j=1}^N[C_jT_j^2(x,t)+\frac{\tau_j}{k_j}q_j^2(x,t)]dx\leqslant e^{t_0}\left\{\int_0^L\sum_{j=1}^N[C_jT_j^2(x,0)+\frac{\tau_j}{k_j}q_j^2(x,0)z]dx+\int_0^t\int_0^L\sum_{j=1}^N\frac{1}{C_j}Q_j^2(x,s)dxds\right\}, \tag{20}$$

for $0\leqslant t\leqslant t_0$ and t_0 is a constant.

Eq. (20) implies that the solutions are dependent upon the initial conditions and the heat sources, and hence the hyperbolic model is well-posed based on the definition given in [31].

3. Finite difference scheme

To develop a stable finite difference scheme, which satisfies a discrete analogue of Eq. (20), we first design a staggered grid where $\{T_j\}_{j=1}^N$ and $\{q_j\}_{j=1}^N$ are placed at different locations, as shown in Fig. 2. Here, $(T_j)_m^n$ and $(q_j)_m^n$ are denoted as the numerical approximations of $T_j((m-\frac{1}{2})\Delta x,n\Delta t)$ and $q_j(m\Delta x,n\Delta t)$, respectively, where Δx and Δt are the x-directional spatial and temporal mesh sizes, respectively, and $1\leqslant m\leqslant M$ for T_j and $1\leqslant m\leqslant M+1$ for q_j, so that $M\Delta x=L$. Furthermore, the first-order forward and backward finite difference operators are defined as

$$\nabla_x u_m=\frac{u_{m+1}-u_m}{\Delta x},\quad \nabla_{\bar{x}}u_m=\frac{u_m-u_{m-1}}{\Delta x}.$$

Thus, a Crank–Nicholson type of finite difference scheme for solving Eqs. (7–9), in one dimension can be developed as

$$C_1\frac{(T_1)_m^{n+1}-(T_1)_m^n}{\Delta t}=\nabla_x\left[\frac{(q_1)_m^{n+1}+(q_1)_m^n}{2}\right]-\sum_{i=2}^N G_{1i}\left[\frac{(T_1)_m^{n+1}+(T_1)_m^n}{2}-\frac{(T_i)_m^{n+1}+(T_i)_m^n}{2}\right]+(Q_1)_m^{n+\frac{1}{2}}, \tag{21a}$$

$$\tau_1\frac{(q_1)_m^{n+1}-(q_1)_m^n}{\Delta t}+\frac{(q_1)_m^{n+1}+(q_1)_m^n}{2}=-k_1\nabla_{\bar{x}}\left(\frac{(T_1)_m^{n+1}+(T_1)_m^n}{2}\right), \tag{21b}$$

$$C_j\frac{(T_j)_m^{n+1}-(T_j)_m^n}{\Delta t}=\nabla_x\left[\frac{(q_j)_m^{n+1}+(q_j)_m^n}{2}\right]+\sum_{i=1}^{j-1}G_{ij}\left[\frac{(T_i)_m^{n+1}+(T_i)_m^n}{2}-\frac{(T_j)_m^{n+1}+(T_j)_m^n}{2}\right]-\sum_{i=j+1}^N G_{ji}\left[\frac{(T_j)_m^{n+1}+(T_j)_m^n}{2}-\frac{(T_i)_m^{n+1}+(T_i)_m^n}{2}\right]+(Q_j)_m^{n+\frac{1}{2}}, \tag{22a}$$

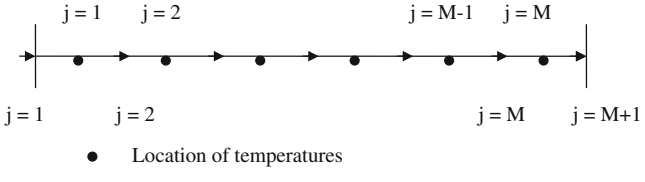

Fig. 2. Configuration of a staggered grid.

$$\tau_j\frac{(q_j)_m^{n+1}-(q_j)_m^n}{\Delta t}+\frac{(q_j)_m^{n+1}+(q_j)_m^n}{2}=-k_j\nabla_{\bar{x}}\left(\frac{(T_j)_m^{n+1}+(T_j)_m^n}{2}\right),\quad j=2,\ldots,N-1, \tag{22b}$$

$$C_N\frac{(T_N)_m^{n+1}-(T_N)_m^n}{\Delta t}=\nabla_x\left[\frac{(q_N)_m^{n+1}+(q_N)_m^n}{2}\right]+\sum_{i=1}^{N-1}G_{iN}\left[\frac{(T_i)_m^{n+1}+(T_i)_m^n}{2}-\frac{(T_N)_m^{n+1}+(T_N)_m^n}{2}\right]+(Q_N)_m^{n+\frac{1}{2}}, \tag{23a}$$

$$\tau_N\frac{(q_N)_m^{n+1}-(q_N)_m^n}{\Delta t}+\frac{(q_N)_m^{n+1}+(q_N)_m^n}{2}=-k_N\nabla_{\bar{x}}\left(\frac{(T_N)_m^{n+1}+(T_N)_m^n}{2}\right), \tag{23b}$$

where $1\leqslant m\leqslant M$ for Eqs. (21a), (22a) and (23a), and $2\leqslant m\leqslant M$ for Eqs. (21b), (22b) and (23b). It can be seen that the truncation error of the above scheme at grid points $((m-\frac{1}{2})\Delta x,n\Delta t)$ for T_j and $(m\Delta x,n\Delta t)$ for q_j is $O(\Delta t^2+\Delta x^2)$. The initial and boundary conditions are given as

$$(T_j)_m^0=T_j^0\left(\left(m-\frac{1}{2}\right)\Delta x\right),\quad (q_j)_m^0=q_j^0(m\Delta x), \tag{24a}$$

$$(q_j)_0^n=(q_j)_{M+1}^n=0, \tag{24b}$$

for any time level n, where $1\leqslant m\leqslant M$ for T_j and $1\leqslant m\leqslant M+1$ for q_j, and $j=1,\ldots,N$.

To obtain a discrete energy estimate which is an analogue of Eq. (20), we multiply Eq. (21a) by $\Delta x\frac{(T_1)_m^{n+1}+(T_1)_m^n}{2}$, Eq. (22a) by $\Delta x\frac{(T_j)_m^{n+1}+(T_j)_m^n}{2}$, and Eq. (23a) by $\Delta x\frac{(T_N)_m^{n+1}+(T_N)_m^n}{2}$, sum m over $1\leqslant m\leqslant M$, and then add the results together with respect to j. This gives

$$\begin{aligned}&\frac{\Delta x}{\Delta t}\sum_{j=1}^{N}\frac{C_j}{2}\sum_{m=1}^{M}\left\{[(T_j)_m^{n+1}]^2-[(T_j)_m^n]^2\right\}\\&=-\Delta x\sum_{j=1}^{N}\sum_{m=1}^{M}\nabla_x\left[\frac{(q_j)_m^{n+1}+(q_j)_m^n}{2}\right]\left[\frac{(T_j)_m^{n+1}+(T_j)_m^n}{2}\right]\\&\quad-\Delta x\sum_{\substack{i=1\\i<j}}^{N-1}\sum_{m=1}^{M}G_{ij}\left[\frac{(T_i)_m^{n+1}+(T_i)_m^n}{2}-\frac{(T_j)_m^{n+1}+(T_j)_m^n}{2}\right]^2\\&\quad+\Delta x\sum_{j=1}^{N}\sum_{m=1}^{M}(Q_j)_m^{n+\frac{1}{2}}\frac{(T_j)_m^{n+1}+(T_j)_m^n}{2}.\end{aligned} \tag{25}$$

Using the summation by parts, Eq. (24b), and then Eqs. (21b), (22b) and (23b), we can simplify the first term on the right-hand-side of Eq. (25) as follows:

$$\begin{aligned}\text{First Term}&=-\Delta x\sum_{j=1}^{N}\sum_{m=1}^{M}\left[\frac{(q_j)_{m+1}^{n+1}+(q_j)_{m+1}^n}{2\Delta x}\right]\left[\frac{(T_j)_m^{n+1}+(T_j)_m^n}{2}\right]\\&\quad+\Delta x\sum_{j=1}^{N}\sum_{m=1}^{M}\left[\frac{(q_j)_m^{n+1}+(q_j)_m^n}{2\Delta x}\right]\left[\frac{(T_j)_m^{n+1}+(T_j)_m^n}{2}\right]\\&=-\Delta x\sum_{j=1}^{N}\sum_{m=2}^{M+1}\left[\frac{(q_j)_m^{n+1}+(q_j)_m^n}{2\Delta x}\right]\left[\frac{(T_j)_{m-1}^{n+1}+(T_j)_{m-1}^n}{2}\right]\\&\quad+\Delta x\sum_{j=1}^{N}\sum_{m=1}^{M}\left[\frac{(q_j)_m^{n+1}+(q_j)_m^n}{2\Delta x}\right]\left[\frac{(T_j)_m^{n+1}+(T_j)_m^n}{2}\right]\\&=-\Delta x\sum_{j=1}^{N}\sum_{m=2}^{M}\left[\frac{(q_j)_m^{n+1}+(q_j)_m^n}{2}\right]\left[\frac{(T_j)_{m-1}^{n+1}+(T_j)_{m-1}^n}{2\Delta x}\right]\\&\quad+\Delta x\sum_{j=1}^{N}\sum_{m=2}^{M}\left[\frac{(q_j)_m^{n+1}+(q_j)_m^n}{2}\right]\left[\frac{(T_j)_m^{n+1}+(T_j)_m^n}{2\Delta x}\right]\\&=\Delta x\sum_{j=1}^{N}\sum_{m=2}^{M}\left[\frac{(q_j)_m^{n+1}+(q_j)_m^n}{2}\right]\nabla_{\bar{x}}\left[\frac{(T_j)_m^{n+1}+(T_j)_m^n}{2}\right]\\&=-\Delta x\sum_{j=1}^{N}\sum_{m=2}^{M}\left[\frac{(q_j)_m^{n+1}+(q_j)_m^n}{2}\right]\\&\quad\times\left[\frac{\tau_j}{k_j}\frac{(q_j)_m^{n+1}-(q_j)_m^n}{\Delta t}+\frac{(q_j)_m^{n+1}+(q_j)_m^n}{2k_j}\right]\\&=-\Delta x\sum_{j=1}^{N}\sum_{m=2}^{M}\frac{\tau_j}{2k_j\Delta t}\left\{\left[(q_j)_m^{n+1}\right]^2-[(q_j)_m^n]^2\right\}\\&\quad-\Delta x\sum_{j=1}^{N}\sum_{m=2}^{M}\frac{1}{4k_j}\left\{[(q_j)_m^{n+1}]^2+[(q_j)_m^n]^2\right\}.\end{aligned} \tag{26}$$

Furthermore, by the Cauchy–Schwarz inequality, we have

$$\begin{aligned}&\Delta x\sum_{j=1}^{N}\sum_{m=1}^{M}(Q_j)_m^{n+\frac{1}{2}}\frac{(T_j)_m^{n+1}+(T_j)_m^n}{2}\\&=\frac{1}{2}\Delta x\sum_{j=1}^{N}\sum_{m=1}^{M}(Q_j)_m^{n+\frac{1}{2}}(T_j)_m^{n+1}+\frac{1}{2}\Delta x\sum_{j=1}^{N}\sum_{m=1}^{M}(Q_j)_m^{n+\frac{1}{2}}(T_j)_m^n\\&\leqslant\frac{1}{4}\Delta x\sum_{j=1}^{N}\sum_{m=1}^{M}C_j[(T_j)_m^{n+1}]^2+\frac{1}{4}\Delta x\sum_{j=1}^{N}\sum_{m=1}^{M}\frac{1}{C_j}[(Q_j)_m^{n+\frac{1}{2}}]^2\\&\quad+\frac{1}{4}\Delta x\sum_{j=1}^{N}\sum_{m=1}^{M}C_j[(T_j)_m^n]^2+\frac{1}{4}\Delta x\sum_{j=1}^{N}\sum_{m=1}^{M}\frac{1}{C_j}[(Q_j)_m^{n+\frac{1}{2}}]^2\\&\leqslant\frac{1}{4}\Delta x\sum_{j=1}^{N}\sum_{m=1}^{M}C_j\left\{[(T_j)_m^{n+1}]^2+[(T_j)_m^n]^2\right\}+\frac{\Delta x}{2}\sum_{j=1}^{N}\sum_{m=1}^{M}\frac{1}{C_j}\\&\quad\times[(Q_j)_m^{n+\frac{1}{2}}]^2.\end{aligned} \tag{27}$$

Substituting Eqs. (26) and (27) into Eq. (25) and then multiplying by 2 give

$$\begin{aligned}&\frac{\Delta x}{\Delta t}\sum_{j=1}^{N}C_j\sum_{m=1}^{M}\left\{[(T_j)_m^{n+1}]^2-[(T_j)_m^n]^2\right\}\\&\quad+\Delta x\sum_{j=1}^{N}\sum_{m=2}^{M}\frac{\tau_j}{k_j\Delta t}\left\{[(q_j)_m^{n+1}]^2-[(q_j)_m^n]^2\right\}\\&\quad+\Delta x\sum_{j=1}^{N}\sum_{m=2}^{M}\frac{1}{2k_j}\left\{[(q_j)_m^{n+1}]^2+[(q_j)_m^n]^2\right\}\\&\quad+2\Delta x\sum_{\substack{i=1\\i<j}}^{N}\sum_{m=1}^{M}G_{ij}\left[\frac{(T_i)_m^{n+1}+(T_i)_m^n}{2}-\frac{(T_j)_m^{n+1}+(T_j)_m^n}{2}\right]^2\leqslant\frac{1}{2}\Delta x\\&\quad\times\sum_{j=1}^{N}\sum_{m=1}^{M}C_j\left\{[(T_j)_m^{n+1}]^2+[(T_j)_m^n]^2\right\}+\Delta x\sum_{j=1}^{N}\sum_{m=1}^{M}\frac{1}{C_j}\left[(Q_j)_m^{n+\frac{1}{2}}\right]^2.\end{aligned} \tag{28}$$

Taking out the third and fourth terms on the LHS of Eq. (28) since they are non-negative, one may simplify Eq. (28) as

$$\begin{aligned}&\Delta x\sum_{j=1}^{N}C_j\sum_{m=1}^{M}\left[(T_j)_m^{n+1}\right]^2-\Delta x\sum_{j=1}^{N}C_j\sum_{m=1}^{M}[(T_j)_m^n]^2\\&\quad+\Delta x\sum_{j=1}^{N}\sum_{m=2}^{M}\frac{\tau_j}{k_j\Delta t}\left[(q_j)_m^{n+1}\right]^2-\Delta x\sum_{j=1}^{N}\sum_{m=2}^{M}\frac{\tau_j}{k_j\Delta t}[(q_j)_m^n]^2\end{aligned}$$

$$\leqslant \frac{\Delta t}{2}\Delta x\sum_{j=1}^{N}\sum_{m=1}^{M}C_j\left\{\left[(T_j)_m^{n+1}\right]^2+\left[(T_j)_m^{n}\right]^2\right\}$$
$$+\Delta t\Delta x\sum_{j=1}^{N}\sum_{m=1}^{M}\frac{1}{C_j}\left[(Q_j)_m^{n+\frac{1}{2}}\right]^2. \tag{29}$$

If we denote $\tilde{F}(n)=\Delta x\sum_{j=1}^{N}C_j\sum_{m=1}^{M}[(T_j)_m^n]^2+\Delta x\sum_{j=1}^{N}\sum_{m=2}^{M}\frac{\tau_j}{k_j\Delta t}[(q_j)_m^n]^2$ and $\tilde{Q}(n+1)=\Delta x\sum_{j=1}^{N}\sum_{m=1}^{M}\frac{1}{C_j}[(Q_j)_m^{n+\frac{1}{2}}]^2$, then Eq. (29) can be further simplified as follows:

$$\left(1-\frac{\Delta t}{2}\right)\tilde{F}(n+1)\leqslant\left(1+\frac{\Delta t}{2}\right)\tilde{F}(n)+\Delta t\tilde{Q}(n+1). \tag{30}$$

Thus, we obtain from Eq. (30) that

$$\begin{aligned}\tilde{F}(n)&\leqslant\frac{1+\frac{\Delta t}{2}}{1-\frac{\Delta t}{2}}\tilde{F}(n-1)+\frac{\Delta t}{1-\frac{\Delta t}{2}}\tilde{Q}(n)\\&\leqslant\frac{1+\frac{\Delta t}{2}}{1-\frac{\Delta t}{2}}\left[\frac{1+\frac{\Delta t}{2}}{1-\frac{\Delta t}{2}}\tilde{F}(n-2)+\frac{\Delta t}{1-\frac{\Delta t}{2}}\tilde{Q}(n-1)\right]\\&\quad+\frac{\Delta t}{1-\frac{\Delta t}{2}}\tilde{Q}(n)\leqslant\cdots\leqslant\left(\frac{1+\frac{\Delta t}{2}}{1-\frac{\Delta t}{2}}\right)^n\tilde{F}(0)\\&\quad+\frac{\Delta t}{1-\frac{\Delta t}{2}}\left[1+\left(\frac{1+\frac{\Delta t}{2}}{1-\frac{\Delta t}{2}}\right)+\left(\frac{1+\frac{\Delta t}{2}}{1-\frac{\Delta t}{2}}\right)^2+\cdots+\left(\frac{1+\frac{\Delta t}{2}}{1-\frac{\Delta t}{2}}\right)^{n-1}\right]\max_{0\leqslant k\leqslant n}\tilde{Q}(k)\\&=\left(\frac{1+\frac{\Delta t}{2}}{1-\frac{\Delta t}{2}}\right)^n\tilde{F}(0)+\frac{\Delta t}{1-\frac{\Delta t}{2}}\left[\frac{1-(\frac{1+\frac{\Delta t}{2}}{1-\frac{\Delta t}{2}})^n}{1-\left(\frac{1+\frac{\Delta t}{2}}{1-\frac{\Delta t}{2}}\right)}\right]\max_{0\leqslant k\leqslant n}\tilde{Q}(k)\\&=\left(\frac{1+\frac{\Delta t}{2}}{1-\frac{\Delta t}{2}}\right)^n\tilde{F}(0)-\left[1-\left(\frac{1+\frac{\Delta t}{2}}{1-\frac{\Delta t}{2}}\right)^n\right]\max_{0\leqslant k\leqslant n}\tilde{Q}(k)\\&\leqslant\left(\frac{1+\frac{\Delta t}{2}}{1-\frac{\Delta t}{2}}\right)^n[\tilde{F}(0)+\max_{0\leqslant k\leqslant n}\tilde{Q}(k)].\end{aligned} \tag{31}$$

Using the inequalities $(1+\varepsilon)^n\leqslant e^{n\varepsilon}$ for $\varepsilon>0$, and $(1-\varepsilon)^{-1}\leqslant e^{2\varepsilon}$ when $0<\varepsilon\leqslant\frac{1}{2}$, we obtain for sufficiently small Δt

$$\tilde{F}(n)\leqslant e^{n\frac{\Delta t}{2}}\cdot e^{n\Delta t}[\tilde{F}(0)+\max_{0\leqslant k\leqslant n}\tilde{Q}(k)]\leqslant e^{\frac{3n\Delta t}{2}}[\tilde{F}(0)+\max_{0\leqslant k\leqslant n}\tilde{Q}(k)]. \tag{32}$$

Hence, the solutions of the scheme, Eqs. (21–24) satisfy, when Δt is sufficiently small

$$\begin{aligned}&\Delta x\sum_{j=1}^{N}C_j\sum_{m=1}^{M}[(T_j)_m^n]^2+\Delta x\sum_{j=1}^{N}\sum_{m=2}^{M}\frac{\tau_j}{k_j\Delta t}[(q_j)_m^n]^2\\&\leqslant e^{\frac{3}{2}n\Delta t}\cdot\left\{\Delta x\sum_{j=1}^{N}C_j\sum_{m=1}^{M}[(T_j)_m^0]^2+\Delta x\sum_{j=1}^{N}\sum_{m=2}^{M}\frac{\tau_j}{k_j\Delta t}[(q_j)_m^0]^2\right.\\&\quad\left.+\max_{0\leqslant k\leqslant n}\Delta x\sum_{j=1}^{N}\sum_{m=1}^{M}\frac{1}{C_j}[(Q_j)_m^{k+\frac{1}{2}}]^2\right\},\end{aligned} \tag{33}$$

for any n in $0\leqslant n\Delta t\leqslant t_0$.

Eq. (33) can be considered as a discrete analogue of Eq. (20). Using the discrete energy estimate, one may obtain that the scheme, Eqs. (21–24), is unconditionally stable. Indeed, if we assume that $(T_j)_m^n$ and $(q_j)_m^n$, $(\hat{T}_j)_m^n$ and $(\hat{q}_j)_m^n$ are the numerical solutions obtained based on the different initial conditions, $(T_j)_m^0$ and $(\hat{T}_j)_m^0$, and different heat sources, $(Q_j)_m^{n+\frac{1}{2}}$ and $(\hat{Q}_j)_m^{n+\frac{1}{2}}$, respectively, but the same boundary conditions, then letting $(E_j)_m^n=(T_j)_m^n-(\hat{T}_j)_m^n$, $(\theta_j)_m^n=(q_j)_m^n-(\hat{q}_j)_m^n$ and $(\varepsilon_j)_m^{n+\frac{1}{2}}=(Q_j)_m^{n+\frac{1}{2}}-(\hat{Q}_j)_m^{n+\frac{1}{2}}$, one may see from Eqs. (21–24) that $(E_j)_m^n$, $(\theta_j)_m^n$ and $(\varepsilon_i)_m^{n+\frac{1}{2}}$ satisfy

$$\begin{aligned}C_1\frac{(E_1)_m^{n+1}-(E_1)_m^n}{\Delta t}&=\nabla_x\left[\frac{(\theta_1)_m^{n+1}+(\theta_1)_m^n}{2}\right]\\&\quad-\sum_{i=2}^{N}G_{1i}\left[\frac{(E_1)_m^{n+1}+(E_1)_m^n}{2}-\frac{(E_i)_m^{n+1}+(E_i)_m^n}{2}\right]\\&\quad+(\varepsilon_1)_m^{n+\frac{1}{2}},\end{aligned} \tag{34a}$$

$$\tau_1\frac{(\theta_1)_m^{n+1}-(\theta_1)_m^n}{\Delta t}+\frac{(\theta_1)_m^{n+1}+(\theta_1)_m^n}{2}=-k_1\nabla_{\bar{x}}\left(\frac{(E_1)_m^{n+1}+(E_1)_m^n}{2}\right); \tag{34b}$$

$$\begin{aligned}C_j\frac{(E_j)_m^{n+1}-(E_j)_m^n}{\Delta t}&=\nabla_x\left[\frac{(\theta_j)_m^{n+1}+(\theta_j)_m^n}{2}\right]\\&\quad+\sum_{i=1}^{j-1}G_{ij}\left[\frac{(E_i)_m^{n+1}+(E_i)_m^n}{2}-\frac{(E_j)_m^{n+1}+(E_j)_m^n}{2}\right]\\&\quad-\sum_{i=j+1}^{N}G_{ji}\left[\frac{(E_j)_m^{n+1}+(T_j)_m^n}{2}-\frac{(E_i)_m^{n+1}+(E_i)_m^n}{2}\right]\\&\quad+(\varepsilon_j)_m^{n+\frac{1}{2}},\end{aligned} \tag{35a}$$

$$\begin{aligned}&\tau_j\frac{(\theta_j)_m^{n+1}-(\theta_j)_m^n}{\Delta t}+\frac{(\theta_j)_m^{n+1}+(\theta_j)_m^n}{2}\\&\quad=-k_j\nabla_{\bar{x}}\left(\frac{(E_j)_m^{n+1}+(E_j)_m^n}{2}\right),\quad j=2,\ldots,N-1,\end{aligned} \tag{35b}$$

$$\begin{aligned}C_N\frac{(E_N)_m^{n+1}-(E_N)_m^n}{\Delta t}&=\nabla_x\left[\frac{(\theta_N)_m^{n+1}+(\theta_N)_m^n}{2}\right]\\&\quad+\sum_{i=1}^{N-1}G_{iN}\left[\frac{(E_i)_m^{n+1}+(E_i)_m^n}{2}-\frac{(E_N)_m^{n+1}+(E_N)_m^n}{2}\right]\\&\quad+(\varepsilon_N)_m^{n+\frac{1}{2}},\end{aligned} \tag{36a}$$

$$\tau_N\frac{(\theta_N)_m^{n+1}-(\theta_N)_m^n}{\Delta t}+\frac{(\theta_N)_m^{n+1}+(\theta_N)_m^n}{2}=-k_N\nabla_{\bar{x}}\left(\frac{(E_N)_m^{n+1}+(E_N)_m^n}{2}\right), \tag{36b}$$

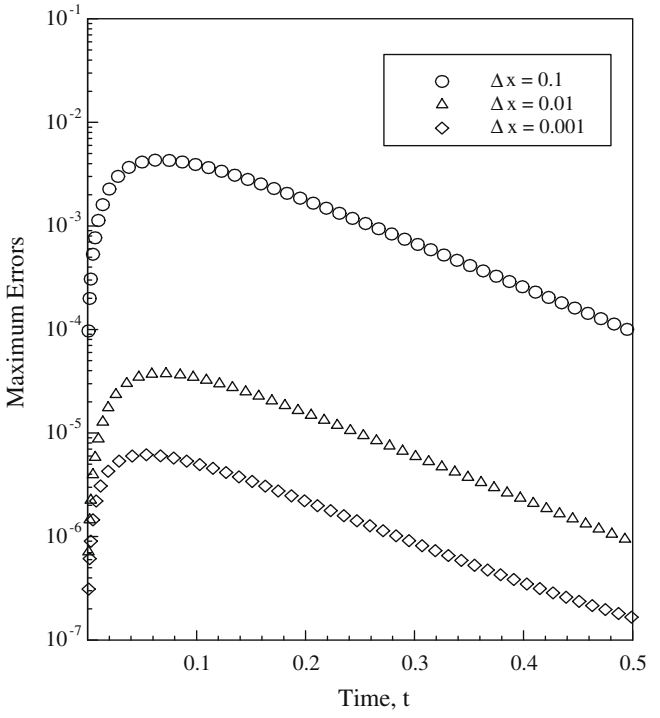

Fig. 3. Maximum errors between numerical solutions of T_1(T_2 and T_3 and the corresponding exact solutions obtained using $\tau_1=\tau_2=\tau_3=0.01$ vs. time.

where $1 \leqslant m \leqslant M$ for Eqs. (34a), (35a) and (36a), and $2 \leqslant m \leqslant M$ for Eqs. (34b), (35b) and (36b) and

$$(E_j)_m^0 = E_j^0\left(\left(m-\frac{1}{2}\right)\Delta x\right), \quad (\theta_j)_m^0 = \theta_j^0(m\Delta x), \tag{37a}$$

$$(\theta_j)_0^n = (\theta_j)_{M+1}^n = 0. \tag{37b}$$

Hence, we conclude from the above derivations that $(E_j)_m^n$, $(\theta_j)_m^n$ and $(\varepsilon_i)_m^{n+\frac{1}{2}}$ should satisfy the discrete energy estimate, Eq. (33)

$$\begin{aligned}&\Delta x\sum_{j=1}^{N} C_j \sum_{m=1}^{M}[(E_j)_m^n]^2 + \Delta x\sum_{j=1}^{N}\sum_{m=2}^{M}\frac{\tau_j}{k_j\Delta t}[(\theta_j)_m^n]^2 \\ &\leqslant e^{\frac{3}{2}t_0}\cdot\left\{\Delta x\sum_{j=1}^{N} C_j\sum_{m=1}^{M}[(E_j)_m^0]^2\right. \\ &\left.+\Delta x\sum_{j=1}^{N}\sum_{m=2}^{M}\frac{\tau_j}{k_j\Delta t}[(\theta_j)_m^0]^2 + \max_{0\leqslant k\leqslant n}\Delta x\sum_{j=1}^{N}\sum_{m=1}^{M}\frac{1}{C_j}[(\varepsilon_j)_m^{k+\frac{1}{2}}]^2\right\},\end{aligned} \tag{38}$$

for any n in $0 \leqslant n\Delta t \leqslant t_0$. Because there is no restriction on the mesh ratio, Eq. (38) implies that the scheme is unconditionally stable with respect to the initial conditions and the heat sources.

4. Numerical example

To see the difference between the parabolic model and hyperbolic model and to test the applicability of the finite difference scheme, we consider a 1D simple three-component system as follows:

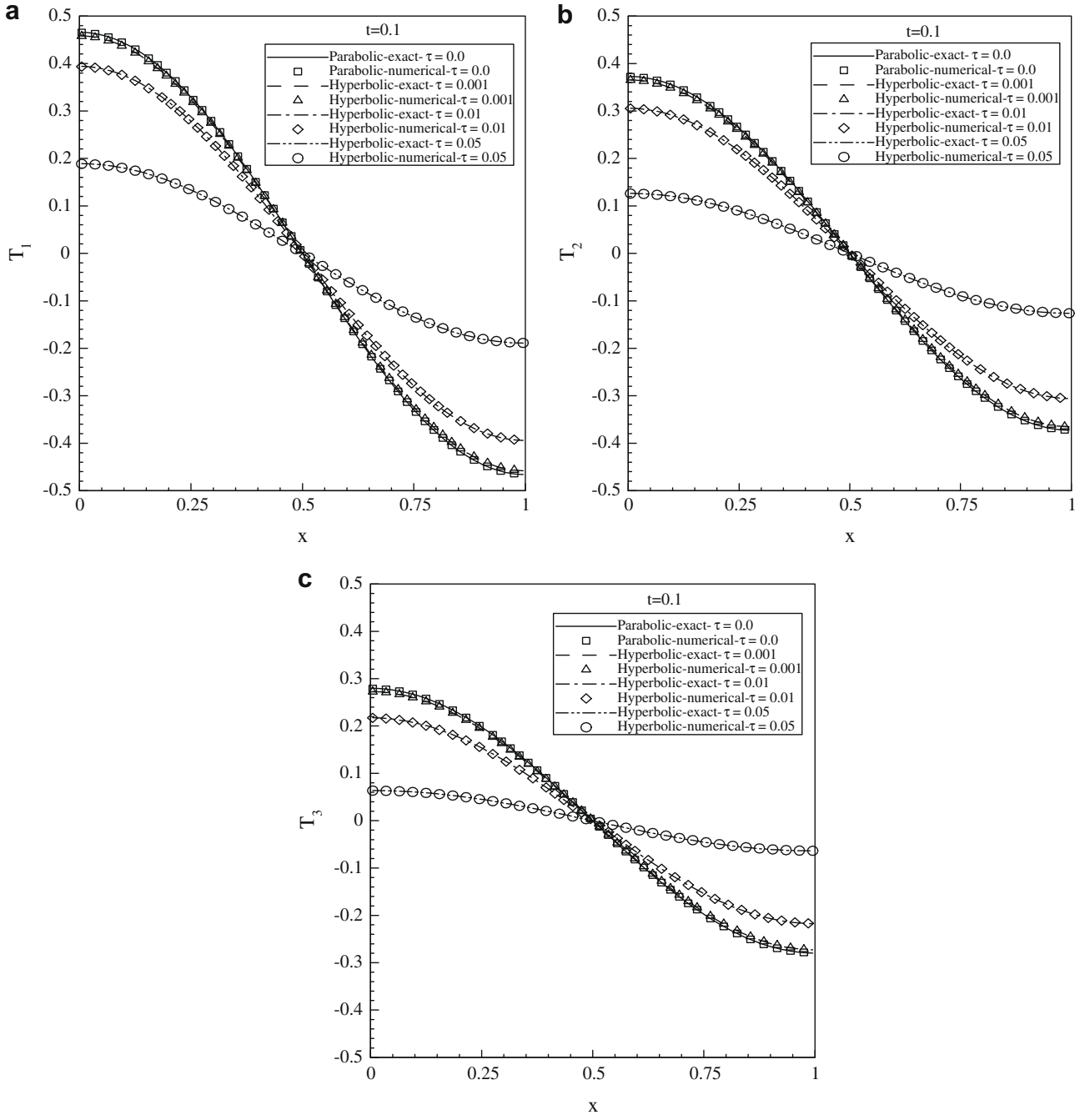

Fig. 4. Numerical solutions (a) T_1, (b) T_2, and (c) T_3, and the corresponding exact solutions at $t = 0.1$ obtained using $\tau_1 = \tau_2 = \tau_3 = \tau = 0.0$, 0.001,0.01, and 0.05.

$$\frac{\partial T_1}{\partial t} = -\frac{\partial q_1}{\partial x} - \pi^2(T_1 - T_2) - \pi^2(T_1 - T_3) + 2\pi^2 e^{-\pi^2 t}\cos \pi x, \quad (39a)$$

$$\tau_1 \frac{\partial q_1}{\partial t} + q_1 = -2\frac{\partial T_1}{\partial x}, \quad (39b)$$

$$\frac{\partial T_2}{\partial t} = -\frac{\partial q_2}{\partial x} + \pi^2(T_1 - T_2) - \pi^2(T_2 - T_3) + \pi^2 e^{-\pi^2 t}\cos \pi x, \quad (40a)$$

$$\tau_2 \frac{\partial q_2}{\partial t} + q_2 = -2\frac{\partial T_2}{\partial x}, \quad (40b)$$

$$\frac{\partial T_3}{\partial t} = -\frac{\partial q_3}{\partial x} + \pi^2(T_1 - T_3) + \pi^2(T_2 - T_3), \quad (41a)$$

$$\tau_3 \frac{\partial q_3}{\partial t} + q_3 = -2\frac{\partial T_3}{\partial x}; \quad (41b)$$

where $0 \leqslant x \leqslant 1$. We choose appropriate initial and boundary conditions so that the exact solutions of the system can be expressed as follows:

$$T_1 = A_1 e^{-\pi^2 t}\cos \pi x, \quad T_2 = A_2 e^{-\pi^2 t}\cos \pi x, \quad T_3 = A_3 e^{-\pi^2 t}\cos \pi x, \quad (42a)$$

$$q_1 = B_1 e^{-\pi^2 t}\sin \pi x, \quad q_2 = B_2 e^{-\pi^2 t}\sin \pi x, \quad q_3 = B_3 e^{-\pi^2 t}\sin \pi x, \quad (42b)$$

where

$$A_1 = \frac{2 + 2d_2 + 3d_3 + 2d_2 d_3}{d_1 d_2 + d_1 d_3 + d_2 d_3 + d_1 d_2 d_3 - 4}, \quad (43a)$$

$$A_2 = \frac{4 + d_1 + 3d_3 + d_1 d_3}{d_1 d_2 + d_1 d_3 + d_2 d_3 + d_1 d_2 d_3 - 4}, \quad (43b)$$

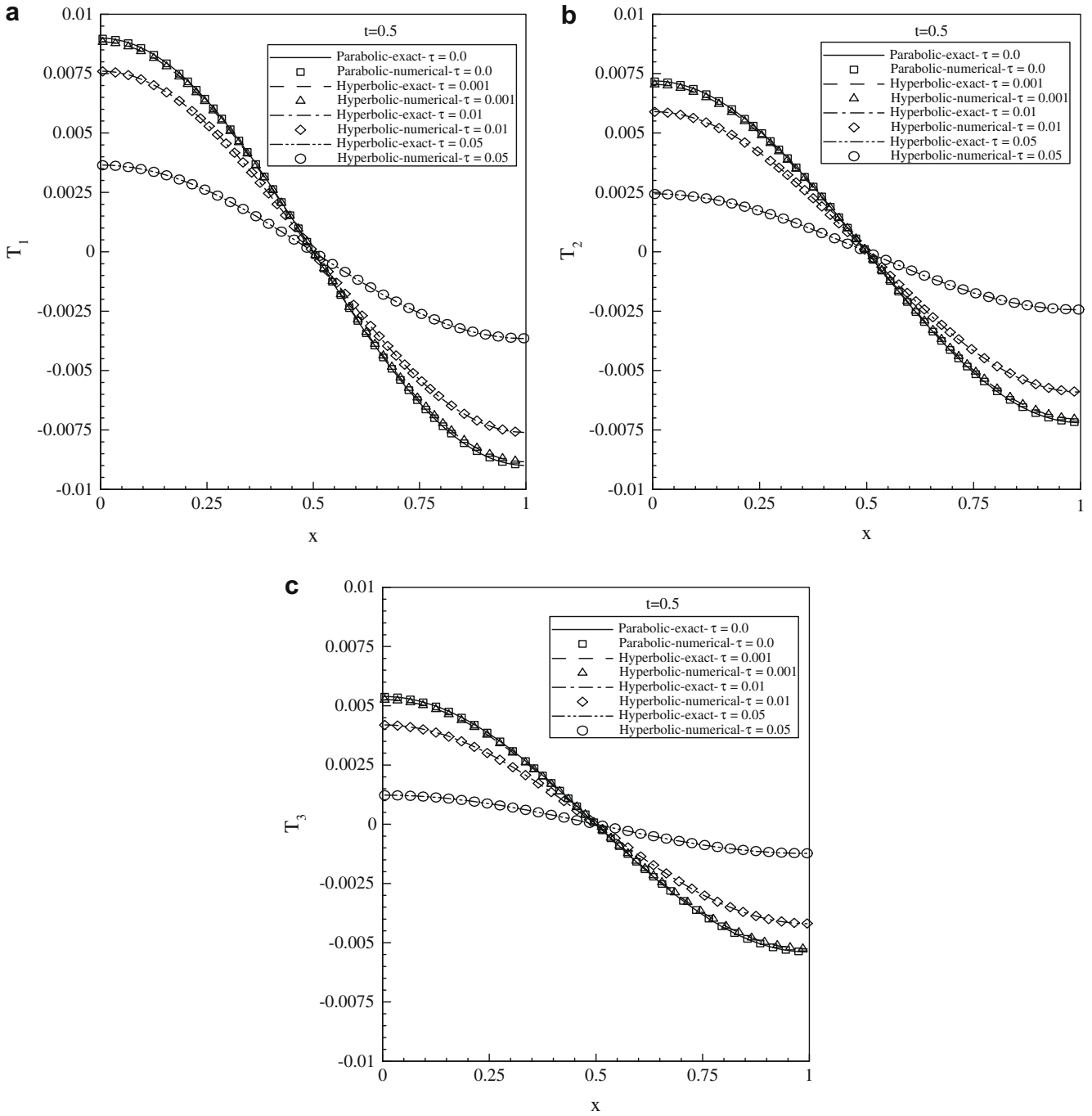

Fig. 5. Numerical solutions (a) T_1, (b) T_2, and (c) T_3, and the corresponding exact solutions at $t = 0.5$ obtained using $\tau_1 = \tau_2 = \tau_3 = \tau = 0.0$, 0.001, 0.01, and 0.05.

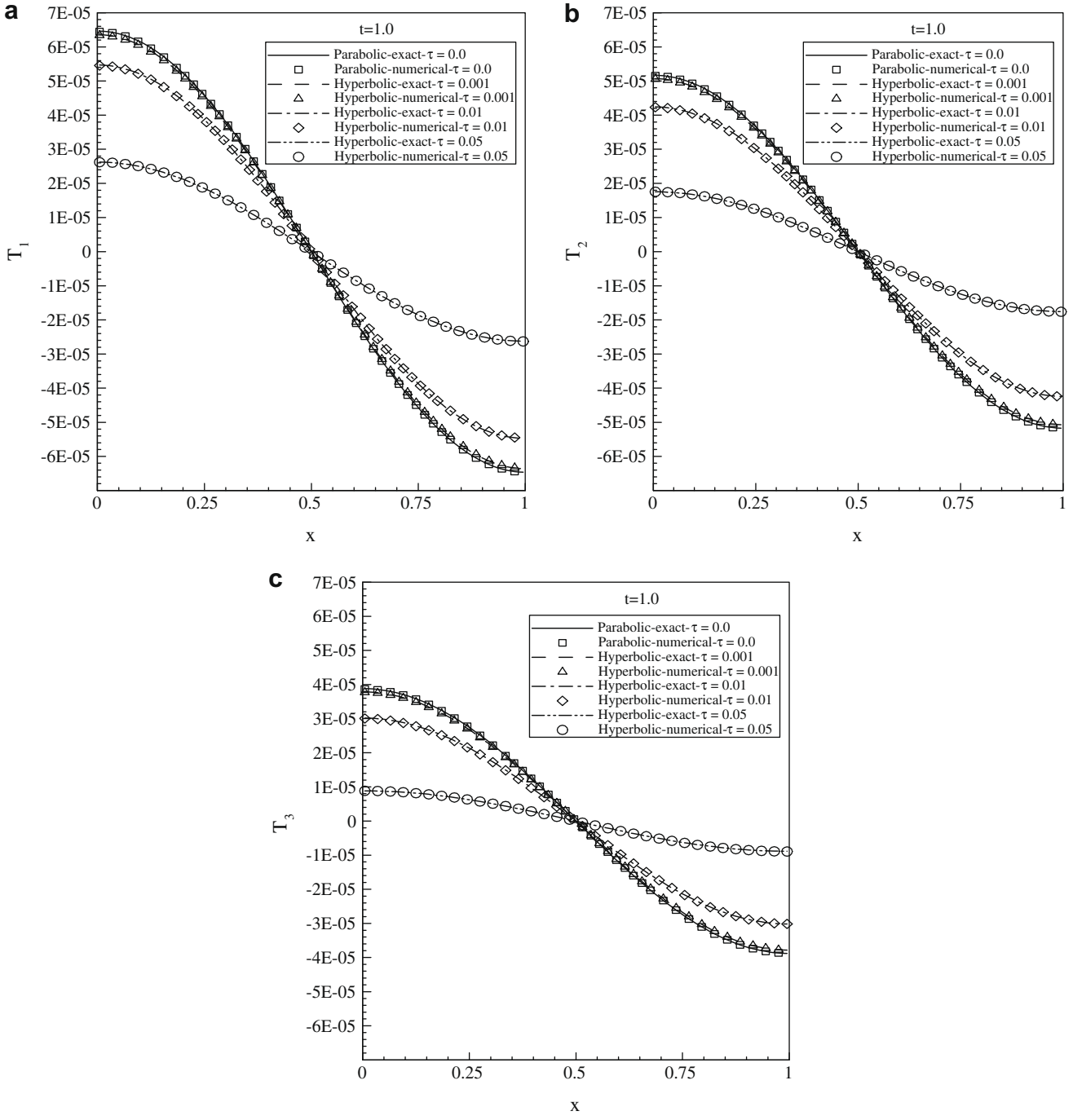

Fig. 6. Numerical solutions (a) T_1, (b) T_2, and (c) T_3, and the corresponding exact solutions at $t = 1.0$ obtained using $\tau_1 = \tau_2 = \tau_3 = \tau = 0.0$, 0.001,0.01, and 0.05.

$$A_3 = \frac{6 + d_1 + 2d_2 + 6d_3 + d_1d_3 + 2d_2d_3}{(1+d_3)(d_1d_2 + d_1d_3 + d_2d_3 + d_1d_2d_3 - 4)}, \tag{43c}$$

$$B_1 = \pi d_1 A_1, \quad B_2 = \pi d_2 A_2, \quad B_3 = \pi d_3 A_3, \tag{43d}$$

$$d_1 = \frac{2}{1-\tau_1\pi^2}, d_2 = \frac{2}{1-\tau_2\pi^2}, \quad d_3 = \frac{2}{1-\tau_3\pi^2}. \tag{43e}$$

It can be seen that the initial and boundary conditions for this example are

$$T_1(x,0) = A_1\cos\pi x, \quad T_2(x,0) = A_2\cos\pi x, \quad T_3(x,0) = A_3\cos\pi x, \tag{44a}$$

$$q_1(x,0) = B_1\sin\pi x, \quad q_2(x,0) = B_2\sin\pi x, \quad q_3(x,0) = B_3\sin\pi x, \tag{44b}$$

$$q_1(0,t) = q_2(x,0) = q_3(x,0) = q_1(1,t) = q_2(1,0) = q_3(1,0) = 0. \tag{44c}$$

Furthermore, when τ_1, τ_2 and τ_3 are zero, the hyperbolic model will reduce to the corresponding parabolic model and the solutions become $T_1 = \frac{5}{4}e^{-\pi^2 t}\cos\pi x, T_2 = e^{-\pi^2 t}\cos\pi x$, and $T_3 = \frac{3}{4}e^{-\pi^2 t}\cos\pi x$.

We first tested the accuracy of the numerical scheme by choosing $\Delta t = 0.001$ and Δx=0.1,0.01,0.001, respectively. The numerical solutions were obtained by employing a Gauss–Seidel type of iteration coupled with the Thomas algorithm for solving tridiagonal

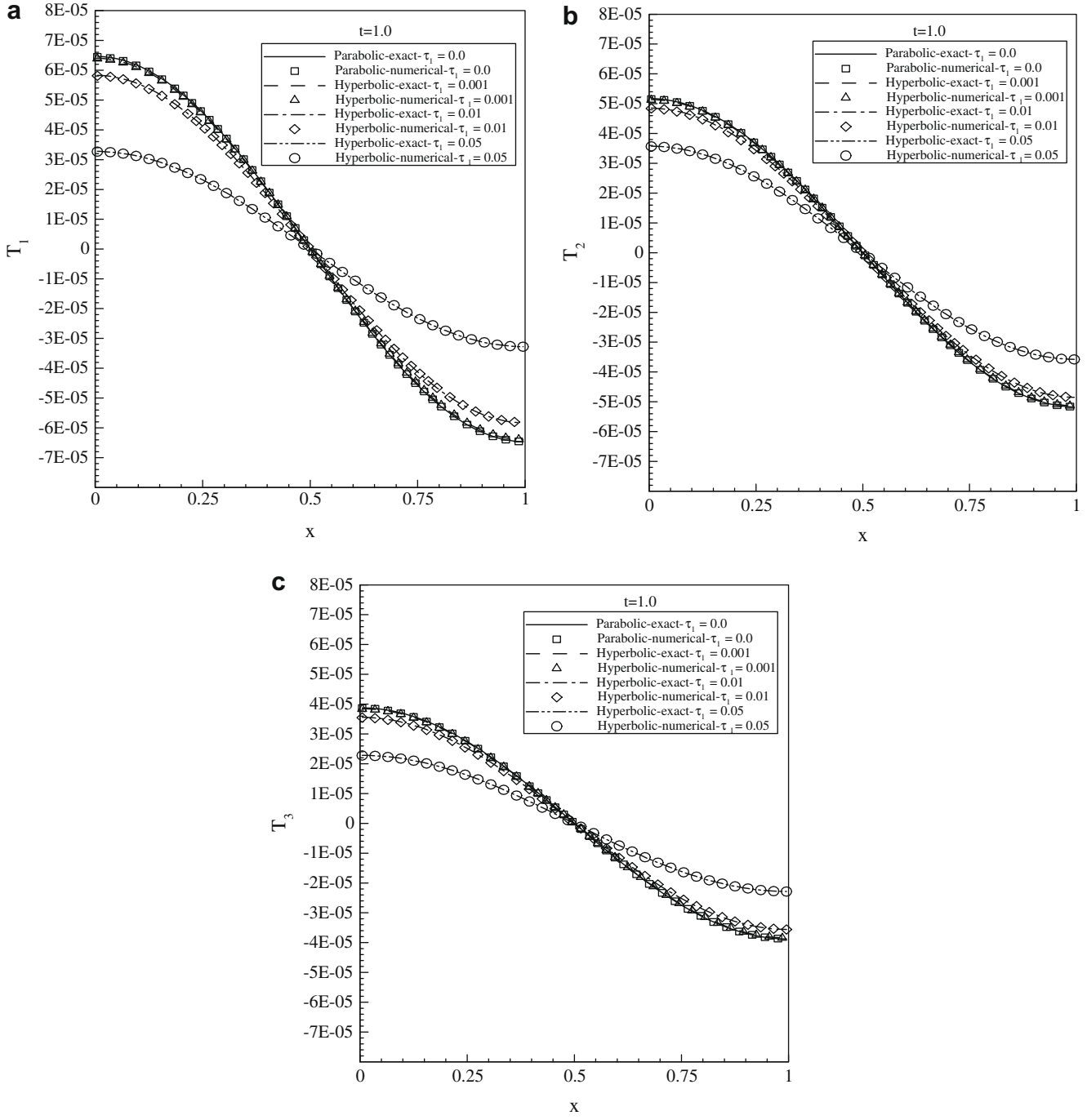

Fig. 7. Numerical solutions (a) T_1, (b) T_2, and (c) T_3, and the corresponding exact solutions at $t = 1.0$ obtained using $\tau_1 = 0.0$, 0.001, 0.01, and 0.05, and $\tau_2 = \tau_3 = 0.0$.

linear systems. The criterion for convergence in our computation was set to be $\max_{j=1,2,3}\max_{1\leqslant m\leqslant M}|(T_j)_m^{n(I+1)} - (T_j)_m^{n(I)}| \leqslant 10^{-12}$, where I is the iterative index. Fig. 3 shows the maximum error between the numerical solutions and the exact solutions at time level $n\max_{j=1,2,3}\max_{1\leqslant m\leqslant M}|(T_j^{\text{numerical}})_m^n - (T_j^{\text{exact}})_m^n|$ vs. time $t(=n\Delta t)$. It can be seen from Fig. 3 that the numerical solutions show to be second-order accurate, as expected.

Figs. 4–6 show the numerical solutions (symbols) of T_1, T_2 and T_3, and the corresponding exact solutions (lines) at $t = 0.1, 0.5, 1.0$, respectively, where $\tau_1 = \tau_2 = \tau_3 = \tau$ was chosen to be 0.0, 0.001, 0.01, and 0.05, respectively. It can be seen from these figures that there are no differences between the numerical solutions and the exact solutions. Similar results can be seen in Fig. 7, where $\tau_1 = 0.0$, 0.001, 0.01, and 0.05, respectively, and $\tau_2 = \tau_3 = 0.0$, at $t = 1.0$, and in Fig. 8 for various values of τ_1, τ_2 and τ_3 at $t = 1.0$. In these computations, we chose $\Delta t = 0.01$ and $\Delta x = 0.01$.

To see the difference between the hyperbolic model and the corresponding parabolic model, we chose the same initial and boundary conditions for both models as follows:

$$T_1(x,0) = \frac{5}{4}\cos \pi x, \quad T_2(x,0) = \cos \pi x, \quad T_3(x,0) = \frac{3}{4}\cos \pi x, \tag{45a}$$

$$q_1(x,0) = \frac{5}{2}\pi \sin \pi x, \quad q_2(x,0) = 2\pi \sin \pi x, \quad q_3(x,0) = \frac{3}{2}\pi \sin \pi x, \tag{45b}$$

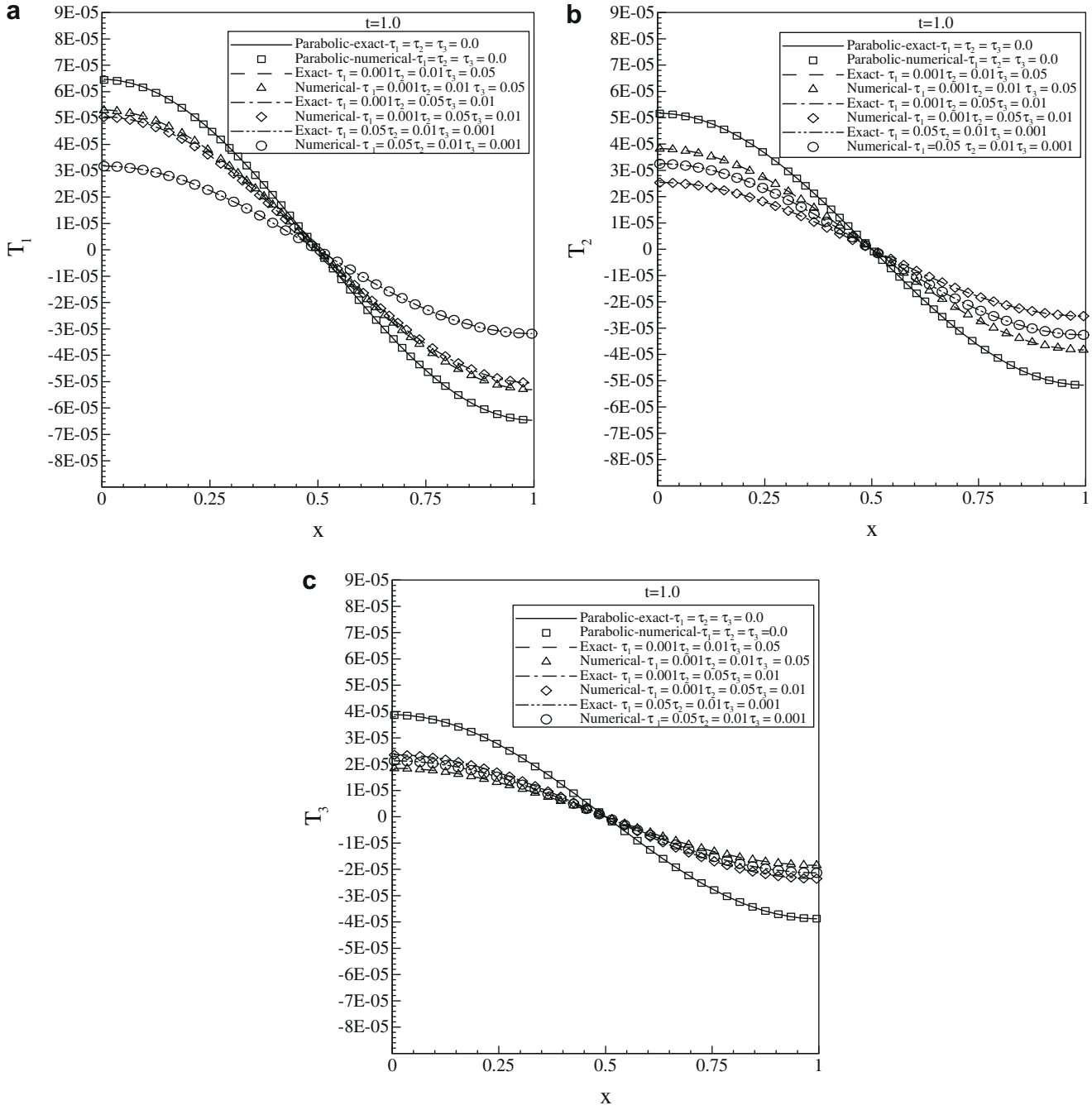

Fig. 8. Numerical solutions (a) T_1, (b) T_2, and (c) T_3, and the corresponding exact solutions at $t = 1.0$ obtained using various values of τ_1, τ_2 and τ_3.

$$q_1(0,t) = q_2(x,0) = q_3(x,0) = q_1(1,t) = q_2(1,0) = q_3(1,0) = 0. \tag{45c}$$

When τ_1, τ_2 and τ_3 are zero, the system, Eqs. (39–41), corresponds to a parabolic model and the exact solutions are $T_1 = \frac{5}{4}e^{-\pi^2 t}\cos \pi x, T_2 = e^{-\pi^2 t}\cos \pi x,$ and $T_3 = \frac{3}{4}e^{-\pi^2 t}\cos \pi x$. On the other hand, when τ_1, τ_2 and τ_3 are not zero, the system, Eqs. (39–41), corresponds to a hyperbolic model. In the computation, we chose $\Delta t = 0.001$ and $\Delta x = 0.001$ with $\tau_1 = \tau_2 = \tau_3 = 0.001$, 0.01 and 0.05, respectively.

Fig. 9 shows the maximum difference between the hyperbolic model and the corresponding parabolic model at time level $n(\max_{j=1,2,3}\max_{1\leqslant m\leqslant M}|(T_j^{\text{hyperbolic}})_m^n - (T_j^{\text{parabolic}})_m^n|)$ vs. time $t(=n\Delta t)$. When $\tau_1 = \tau_2 = \tau_3 = 0.001$, as expected, the solutions obtained by the hyperbolic model are close to those obtained by the parabolic model. However, when $\tau_1 = \tau_2 = \tau_3 = 0.01$ and 0.05, there is a significant difference in solutions between the hyperbolic model and the corresponding parabolic model. It can be seen from Fig. 9 that there is a wave-like difference in solutions between these two models.

5. Conclusion

We have proposed a hyperbolic model for thermal analysis in a generalized *N*-carrier system. The model is shown to satisfy an energy estimate, implying that the model is well-posed. Based on the energy estimate, a finite difference scheme has been developed for solving the hyperbolic model for thermal analysis in the multi-carrier system. The numerical scheme is proven to satisfy a discrete analogue of the energy estimate, implying that it is unconditionally

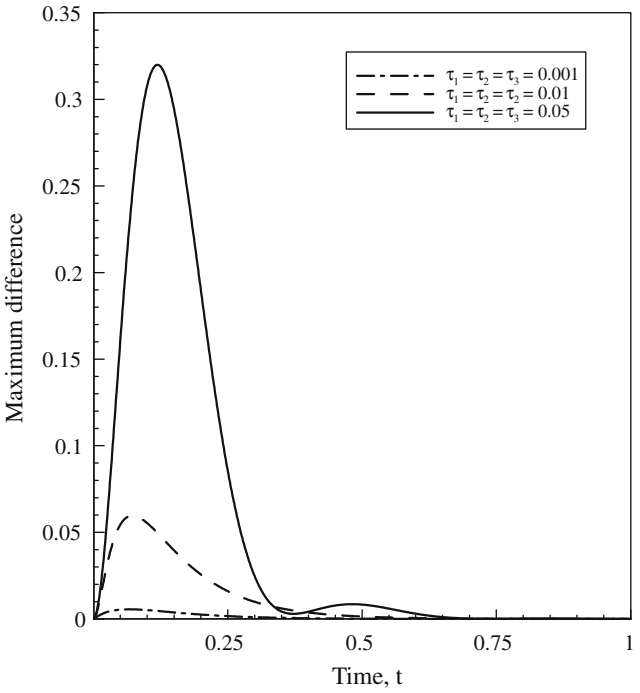

Fig. 9. Maximum difference in solutions between the hyperbolic model and corresponding parabolic model vs.time.

stable. Numerical results show the difference between the hyperbolic model and the corresponding parabolic model. The obtained energy estimate and the numerical scheme in one dimension can be readily generalized to the case of multi-dimensions.

Acknowledgement

The author thanks Professor D.Y. Tzou, Department of Mechanical and Aerospace Engineering, University of Missouri at Columbia, for his valuable suggestions on the *N*-carrier system.

References

[1] M.I. Kaganov, I.M. Lifshitz, M.V. Tanatarov, Relaxation between electrons and crystalline lattices, Sov. Phys. JETP 4 (1957) 173–187.
[2] S.I. Anisimov, B.L. Kapeliovich, T.L. Perel'man, Electron emission from metal surfaces exposed to ultra-short laser pulses, Sov. Phys. JETP 39 (1974) 375–377.
[3] T.Q. Qiu, C.L. Tien, Short-pulse laser heating on metals, Int. J. Heat Mass Transfer 35 (1992) 719–726.
[4] T.Q. Qiu, C.L. Tien, Heat transfer mechanisms during short-pulse laser heating of metals, ASME J. Heat Mass Transfer 115 (1993) 835–841.
[5] D.Y. Tzou, A unified field approach for heat conduction from micro to macroscales, ASME J. Heat Mass Transfer 117 (1995) 8–16.
[6] D.Y. Tzou, Macro- to Microscale Heat Transfer: The Lagging Behavior, Chapter 2, Taylor & Francis, Washington DC, 1997.
[7] W.J. Minkowycz, A. Haji-Sheikhb, K. Vafai, On departure from local thermal equilibrium in porous media due to a rapidly changing heating source: the Sparrow number, Int. J. Heat Mass Transfer 42 (1999) 3373–3385.
[8] D.Y. Tzou, J.K. Chen, Thermal lagging in random media, AIAA J. Thermophys. Heat Transfer 12 (1998) 567–574.
[9] T.Q. Qiu, C.L. Tien, Femtosecond laser heating of multi-layer metals-I analysis, Int. J. Heat Mass Transfer 37 (1994) 2789–2797.
[10] P.J. Antaki, Importance of nonequilibrium thermal conductivity during short-pulse laser-induced desorption from metals, Int. J. Heat Mass Transfer 45 (2002) 4063–4067.
[11] A.N. Smith, J.L. Hosteler, P.M. Norris, Nonequilibrium heating in metal films: an analytical and numerical analysis, Numer. Heat Transfer Part A 35 (1999) 859–873.
[12] D.Y. Tzou, K.S. Chiu, Temperature-dependent thermal lagging in ultrafast laser heating, Int. J. Heat Mass Transfer 44 (2001) 1725–1734.
[13] W. Dai, G. Li, R. Nassar, L. Shen, An unconditionally stable three level finite difference scheme for solving parabolic two-step micro heat transport equations in a three-dimensional double-layered thin film, Int. J. Numer. Meth. Eng. 59 (2004) 493–509.
[14] W. Dai, T. Zhu, in: A nonlinear finite difference scheme for solving two-step nonlinear parabolic heat transport equations, Lecture Notes in Computer Science, vol. 3314, Springer-Verlag, Heidelberg, 2004, pp. 304–309.
[15] H. Wang, W. Dai, R. Nassar, R.V.N. Melnik, A finite difference method for studying thermal deformation in a thin film exposed to ultrashort-pulsed lasers, Int. J. Heat Mass Transfer 49 (2006) 2712–2723.
[16] H. Wang, W. Dai, R.V.N. Melnik, A finite difference method for studying thermal deformation in a double-layered thin film exposed to ultrashort-pulsed lasers, Int. J. Thermal Sciences 46 (2006) 1179–1196.
[17] H. Wang, W. Dai, L.G. Hewavitharana, A finite difference method for studying thermal deformation in a double-layered thin film with imperfect interfacial contact exposed to ultrashort-pulsed lasers, Int. J. Therm. Sci. 47 (2008) 7–24.
[18] S. Zhang, W. Dai, H. Wang, R.V.N. Melnik, A finite difference method for studying thermal deformation in a 3D thin film exposed to ultrashort pulsed lasers, Int. J. Heat Mass Transfer 51 (2008) 1979–1995.
[19] X. Du, W. Dai, A finite difference method for studying thermal deformation in a 3D micro-sphere exposed to ultrashort pulsed lasers, Numer. Heat Transfer Part A 53 (2008) 457–484.
[20] M.A. Al-Nimr, O.M. Haddad, V.S. Arpaci, Thermal behavior of metal films – a hyperbolic two-step model, Heat Mass Transfer 35 (1999) 459–464.
[21] M.A. Al-Nimr, V.S. Arpaci, The thermal behavior of thin metal films in the hyperbolic two-step model, Int. J. Heat Mass Transfer 43 (2000) 2021–2028.
[22] M. Al-Odat, M.A. Al-Nimr, M. Hamdan, Thermal stability of superconductors under the effect of a two-dimensional hyperbolic heat conduction model, Int. J. Numer. Methods Heat Fluid Flow 12 (2002) 173–177.
[23] M. Naji, M.A. Al-Nimr, M. Hader, The validity of using the microscopic hyperbolic heat conduction model under as harmonic fluctuating boundary heating source, Int. J. Thermophys. 24 (2003) 545–557.
[24] M.A. Al-Nimr, M.K. Alkam, Overshooting phenomenon in the hyperbolic microscopic heat conduction model, Int. J. Thermophys. 24 (2003) 577–583.
[25] J.K. Chen, J.E. Beraun, Numerical study of ultrashort laser pulse interactions with metal films, Numer. Heat Transfer Part A 40 (2001) 1–20.
[26] J.K. Chen, J.E. Beraun, C.L. Tham, Investigation of thermal response caused by pulsed laser heating, Numer. Heat Transfer Part A 44 (2003) 705–722.
[27] A. Faghri, Y. Zhang, Transport Phenomena in Multiphase Systems, Elsevier, UK, 2006.
[28] F. Dausinger, F. Lichtner, H. Lubatschowdki, Femtosecond Technology for Technical and Medical Applications, Springer-Verlag, Berlin, Germany, 2004.
[29] D.Y. Tzou, Thermal lagging: multi-component systems and thermoelectric coupling, in: Proceedings of the First ASME Micro/Nanoscale Heat Transfer International Conference (MNHT08), Tainan, Taiwan, January 6–9, 2008.
[30] L.C. Evans, Partial Differential Equations, American Mathematical Society, Providence, Rhode Island, 1998.
[31] J.C. Strikwerda, Finite Difference Schemes and Partial Differential Equations, Chapman & Hall, New York, 1989.